An experimental and numerical investigation of under-expanded turbulent jets

A. J. Saddington, N. J. Lawson and K. Knowles
Aeromechanical Systems Group
Cranfield University
Shrivenham, UK

ABSTRACT

The work described here concentrates on under-expanded, axisymmetric turbulent jets issuing into quiescent conditions. Under-expanded turbulent jets are applicable to most aircraft propulsion applications that use convergent nozzles. Experimental studies used laser doppler velocimetry (LDV) and pitot probe measurements along the jet centreline. These measurements were made for two nozzle pressure ratios (2·5 and 4·0) and at various streamwise positions up to 10 nozzle diameters downstream of the nozzle exit plane. A computational fluid dynamics (CFD) model was developed using the Fluent code and utilised the RNG κ–ε two-equation turbulence model. A mesh resolution of approximately one hundredth of nozzle exit diameter was found to be sufficient to establish a mesh independent solution.

Comparison of the jet centreline axial velocity (LDV data) and pressure ratio (pitot probe data) showed good agreement with the CFD model. The correct number of shock cells had been predicted and the shock strength agreed well between the experiments and numerical model. The CFD model was, however, found to over-predict the shock cell length resulting in a longer supersonic core. There was some evidence, based on analysis of the LDV measurements that indicates the presence of swirl and jet unsteadiness, which could contribute to a shortening of the shock cell length. These effects were not modelled in the CFD. Correlation between the LDV and pitot probe measurements was generally good, however, there was some evidence that probe interference may have caused the premature decay of the jet. Overall, this work has indicated the good agreement between a CFD simulation using the RNG κ–ε turbulence model and experimental data when applied to the prediction of the flowfield generated by under-expanded turbulent jets. The suitability of the LDV technique to jet flows with velocities up to 500ms^{-1} has also been demonstrated.

NOMENCLATURE

CFD	computational fluid dynamics
D	nozzle exit diameter (0·0294m)
l	mixing length
LDV	laser doppler velocimetry
M	Mach number
NPR	nozzle pressure ratio $\left\{\frac{p_{0c}}{p_a}\right\}$
p	static pressure
p_a	atmospheric static pressure
p_0	total pressure
p_{0c}	settling chamber total pressure
p_{0p}	pitot probe pressure
r	radial distance from nozzle centreline
t	static temperature
T_a	atmospheric static temperature
T_i	turbulence intensity $\left\{\frac{\sqrt{\frac{1}{3}\left(u'^2+v'^2+w'^2\right)}}{V_{ref}}\right\}$
u	axial velocity
u_θ	tangential velocity
v	vertical velocity (see Fig. 4)
V_{ref}	reference velocity (speed of sound)
w	horizontal velocity (see Fig. 4)
x	axial distance from nozzle exit

Paper No. 2825. Manuscript received 27 February 2003, revised version received 15 October 2003, accepted 21 January 2004.

$()'$ e.g. u', fluctuating velocity component
$()_{rms}$ e.g. u_{rms}, rms velocity component
$()_1$ upstream of normal shock
$()_2$ downstream of normal shock

1.0 INTRODUCTION

High-speed, compressible, turbulent jets feature in many important aerospace applications, notably in jet aircraft and rocket propulsion, gas turbine combustion chambers and turbomachinery cooling flows. In many of these applications an understanding of the mixing between the jet and an ambient fluid is critical to their successful design. Specific research areas include jet noise reduction[1], high pressure ratio ejector design[2] and infra-red signature reduction[3].

Most jet powered aircraft operating in the high subsonic and low supersonic flight regimes will use turbofan engines with convergent propulsive nozzles (the performance benefit of using a convergent-divergent nozzle is usually negated by the extra weight and complexity of such systems). If the aforementioned research areas are to progress, there exists a requirement for experimental data on an under-expanded turbulent jet on which to base mixing enhancements.

The increasing use of CFD techniques early in the design cycle leads to a requirement for high-quality experimental data with which to validate a particular model, ideally in the form of velocity and turbulence measurements. Until recently, however, experimental data have been limited to pitot probe measurements within the jet plume and surrounding flowfield[4,5]. This raises difficulties with regard to probe interference, which is especially significant for small-scale experiments where shock-probe interference has the potential to give significant measurement errors. The advent of laser-based measurement techniques (such as LDV) has provided the opportunity to conduct non-intrusive measurements. Previous researchers, however, have found difficulty in obtaining reliable mean velocity data in the shock core region of under-expanded jets. In some cases measurements were not made[6], whereas in others, the rapid velocity changes across the shock cells could not be resolved[7]. This work presents new LDV data characterising an under-expanded turbulent jet in the important supersonic core region. The data are validated against traditional pitot probe data and a CFD model of the jet.

1.1 Axisymmetric jets

The general structure of a turbulent free jet is well documented[8]. For a circular convergent nozzle, three variations of the flow pattern are possible, depending on the nozzle pressure ratio (NPR). The three variations that are traditionally identified are the subsonic jet, the under-expanded jet and the highly under-expanded jet[4].

The subsonic jet (Fig. 1) is characterised by a potential core, an area of constant velocity in which no viscous mixing occurs, surrounded by a region in which mixing between jet and ambient fluid takes place. Several nozzle diameters downstream, the mixing region has spread inward to reach the centreline, and the core region no longer exists. Beyond this point, the mixing region continues to spread as the velocity decays at a rate required to conserve axial momentum. In this portion of the jet, the mean velocity profiles approach a self-similar shape. Such a jet exists in air for isentropic nozzle pressure ratios from 1 to 1·893.

When the sonic, or critical, pressure ratio is reached, a very weak normal shock forms at the nozzle exit. This shock changes rapidly with increasing pressure ratio and at a NPR of approximately 2·0, the familiar pattern of 'shock diamonds' or 'cells' composed of intersecting oblique shocks is established in the core (Fig. 2). This structure exists, for a sonic exit, until the NPR is about 4·0. The term 'moderately under-expanded' is used to denote jets within this pressure ratio interval. Due to the additional expansion required in the unconfined jet flow beyond the nozzle, the boundaries of what was the potential core in the subsonic case are now determined by the requirement of pressure equilibrium between the outermost portion of the flow within the shock structure and the surrounding ambient air. The inward diffusion of the mixing region, however, continues, and ultimately results in the dissipation of the 'shock core'. Downstream of the core, after the jet has become subsonic, the spreading and decay rates would be expected to be those of a wholly subsonic jet.

At NPRs greater than about 4·0, the form of the shock structure in the initial cell begins to change. The oblique shock approaching the nozzle centreline gives too high a flow deflection causing streamlines to approach the centreline of the jet at an angle greater than the maximum possible deflection through an oblique shock at the local (downstream) Mach number. As a consequence, a Mach reflection takes place and a normal shock (or Mach disc) is formed (Fig. 3). Once this occurs, the jet is said to be 'highly under-expanded'. The flow then decays through a structure of oblique shocks. The mixing region surrounds the core as usual, but its radial diffusion is small, with the result that the core of the highly under-expanded jet can be extremely long. Far downstream, the usual subsonic decay takes place.

1.2 Objectives

The objectives of this study were to take LDV velocity measurements in the supersonic core of a jet issuing from a circular convergent nozzle and to compare the data with a CFD model of the experiment. There were two main aims. The first aim was to determine if the LDV technique was suitable for measurements in supersonic flow with shock waves. The second aim was to ascertain the ability of the CFD model to adequately predict the shock cell structure and the length of the shock core. Comparisons were also made between the LDV data, CFD model and previous pitot probe measurements of the same experiment [9,10].

2.0 METHODOLOGY

2.1 Experiments

Experiments were conducted in a nozzle test cell at Shrivenham (Fig. 4). Two Howden rotary screw compressors running in series supplied compressed dried air at a pressure of 6·9 bar (gauge) and a

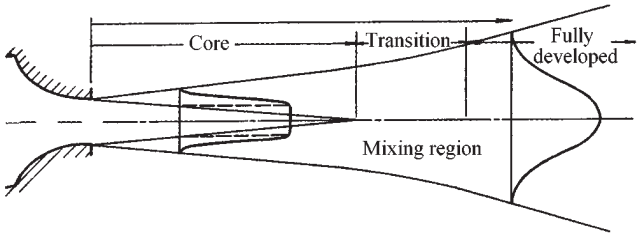

Figure 1. A subsonic free jet[4].

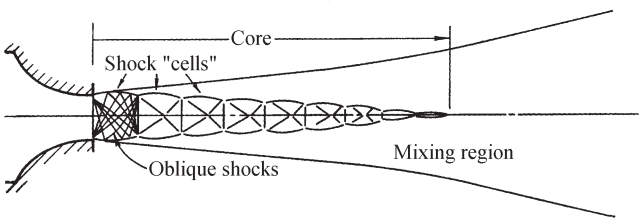

Figure 2. An under-expanded free jet[4].

https://doi.org/10.1017/S0001924000151590 Published online by Cambridge University Press

flow rate of 1·02kgs^{-1} to a small plenum chamber in this cell. For the jet experiments reported here, the compressors were run continuously and discharged to atmosphere, with the required jet air supply being bled off to a 34·4mm internal diameter, 152mm long jet pipe to which test nozzles were attached, in this case an axisymmetric nozzle was used with a 29·4mm exit diameter (Fig. 5).

Jet total pressure, p_{0c} was measured using a pitot tube (within the jet supply pipe) and adjusted with a gate valve, which controlled the proportion of the compressed air supply that was discharged to atmosphere. Using this method, the NPR could be set to an accuracy of ±0·1. Flow temperature was measured with a thermometer mounted indirectly in the jet rig supply pipe. The jet air was exhausted from the test cell through a 0·3m diameter hole via a 45° capture cone, which was 0·42m downstream of the nozzle exit (Fig. 4). Data were collected at NPRs of 2·5 and 4·0.

Three-dimensional LDV measurements were taken using a Dantec system based on FibreFlow optics, two 300mm focal length probes, three BSA enhanced signal processors and Dantec Burstware software. The probes were set up with beam separations of 20mm giving probe volumes of 150μm × 150μm × 2·8mm. The processors were set to non-coincidence mode to ensure acceptable data rates in *u, v* and *w*. Seeding of the jet was by direct injection from a TSI six-jet seeder into the plenum chamber using JEM Hydrosonic seeding fluid.

Measurement traverses were made at 2·5mm intervals along the nozzle centreline, across the nozzle exit plane and across the jet at one, two, five and ten diameters downstream of the exit. Each measurement point was sampled for five seconds and contained between 1,000 and 3,000 samples to yield *u*, *v*, and *w* mean velocities and u_{rms}, v_{rms} and w_{rms} turbulence data. Probe access limited data collection to within 10*D* of the nozzle exit plane. The LDV measurements were estimated to be accurate to ±1% of velocity based on the sample time and frequency.

Additional comparative data were taken from centreline pitot probe measurements made previously under the same test conditions[9,10]. The pitot probe was mounted on a 2*D* travelling microscope carriage modified to accommodate a stepper motor on each axis. The carriage was driven with a traverse range of 120mm. Physical carriage location could be verified using vernier scales mounted on each axis. The traverse plane was parallel to the jet axis enabling centre-line pitot pressure profiles to be obtained. The limited travel of the carriage required the rig to be repositioned downstream to give coverage of the whole jet. Thus, centreline pressure profiles consist of two plots taken at different times. Data points were recorded at 2mm intervals along the jet centreline. Probe access limited the extent of measurements to just under 8*D*.

2.2 Numerical model

The CFD model was developed using the Fluent commercial code (Version 5.5). The computational domain consisted of an axisymmetric structured mesh with approximately 50,000 cells. The boundary condition for the nozzle was set as a pressure inlet with a prescribed total pressure, static pressure, total temperature and turbulence intensity. The turbulence intensity, T_i at nozzle inlet in the CFD model was adjusted to give the same nozzle exit turbulence intensity as the experiments (approximately 4%). The experimental T_i was derived from the rms velocity data measured by the LDV technique. The turbulence length scale was set as 7·5 of nozzle radius[11]. The farfield boundary was set as a pressure outlet with a prescribed static pressure and static temperature. The boundary conditions are summarised in Table 1.

The inlet plane was approximately 1*D* upstream of the nozzle exit (Fig. 6), the outlet plane was at about 50*D* downstream and the radial boundary diverged from 2*D* at the upstream end to more than 10D downstream. Turbulent calculations were performed using the RNG κ–ε turbulence model[12], which has been shown to be suitable for modelling under-expanded jets[13].

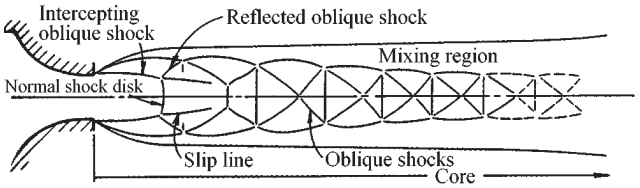

Figure 3. A highly under-expanded free jet[4].

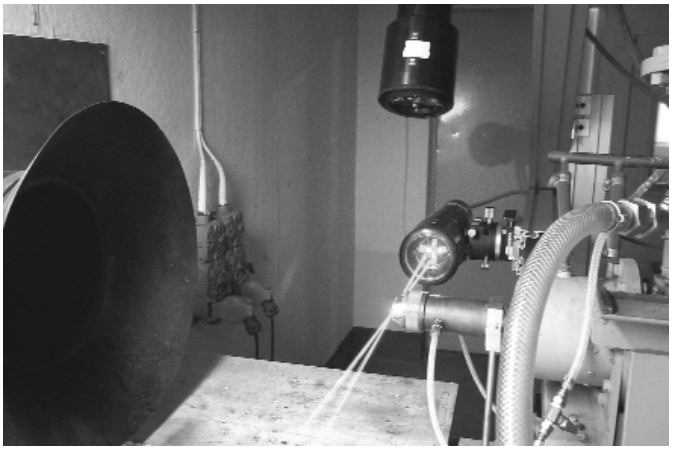

Figure 4. LDV measurements in the nozzle test cell.

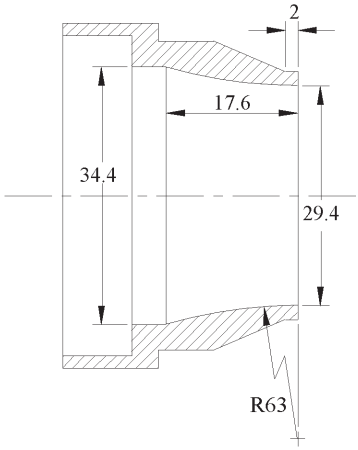

Figure 5. Nozzle geometry showing the internal profile.

Table 1
Summary of the boundary conditions for the CFD model

Boundary condition	Variable	Magnitude
Nozzle inlet	p_0	NPR × p_a
	p	p_a
	T	T_a
	T_i	From LDV
	l	0·075 (*D*/2)
Farfield	p	p_a
	T	T_a

https://doi.org/10.1017/S0001924000151590 Published online by Cambridge University Press

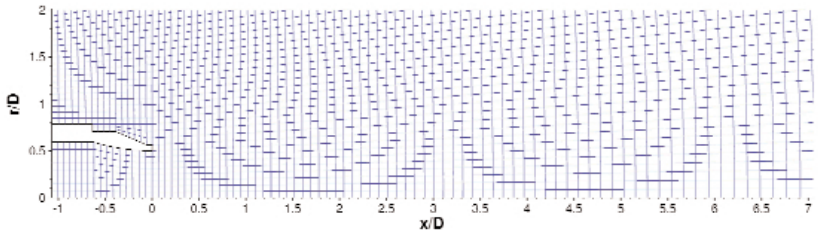

Figure 6. The initial 2D axisymmetric mesh in the nozzle region

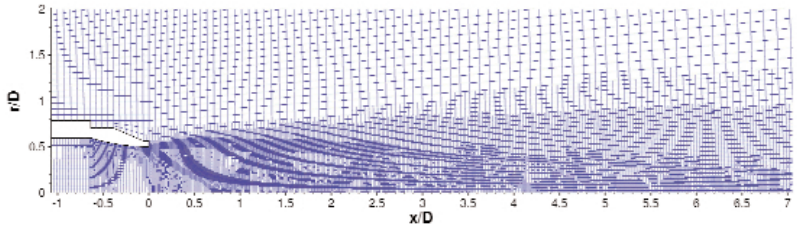

Figure 7. A typical 2D axisymmetric mesh after solution-based grid adaptation.

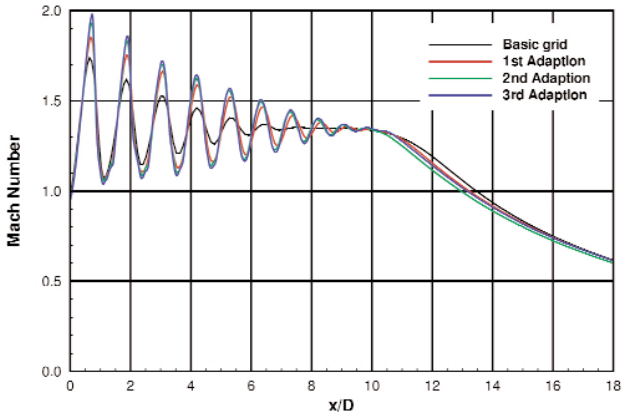

Figure 8. Predicted jet centre-line Mach number profiles – effect of grid refinement (NPR = 3).

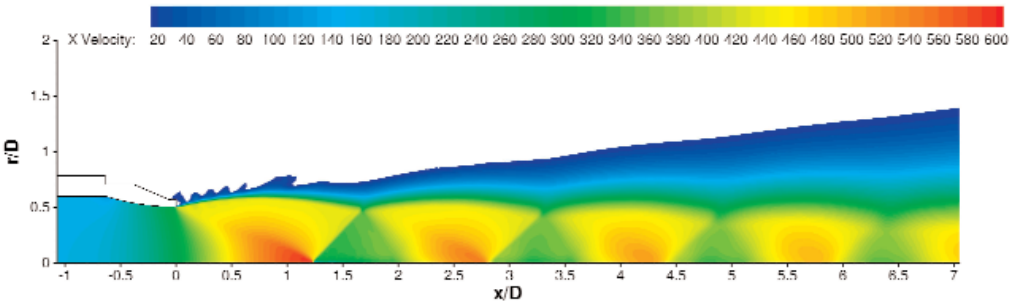

Figure 9. Contours of axial velocity showing the well defined shock structure (NPR = 4).

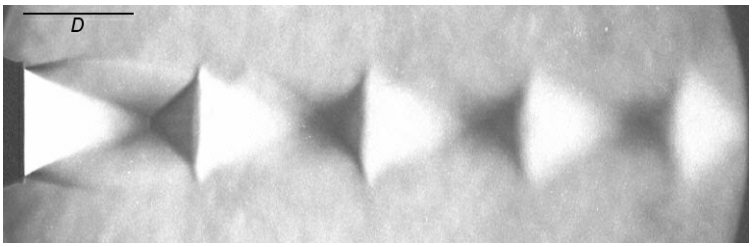

Figure 10. Schlieren flow visualisation of the jet shock structure (NPR = 4).

https://doi.org/10.1017/S0001924000151590 Published online by Cambridge University Press

Initial axisymmetric calculations were conducted on a mesh of 6,600 cells (Fig. 6). Three stages of mesh adaption, based on density gradients greater than 1×10^{-6}, were then performed in order to capture the jet shock structure accurately. This increased the grid resolution in the shock cell regions from 2mm to 0·25mm (Fig. 7).

Figure 8 shows centreline Mach number profiles for the initial mesh and the three stages of mesh adaption. The solution is clearly improved by the solution-based adaption, particularly after the first stage. Further improvement in the shock cell definition is seen in the second and third stages of adaption but by the third stage the incremental change is small. It was concluded, therefore, that three stages of mesh adaption were sufficient to ensure a mesh-independent solution. The solution-based mesh adaption gave a well defined shock structure (Fig. 9) without the expense of having an excessively fine mesh over the whole of the solution domain. This compares well with previous schlieren flow visualisation images of an axisymmetric jet from the same nozzle[10] (Fig. 10).

Calculations were performed using a multi-stage (Runge-Kutta) solver employing a full approximation storage multi-grid scheme with five levels to accelerate the multi-stage solver.

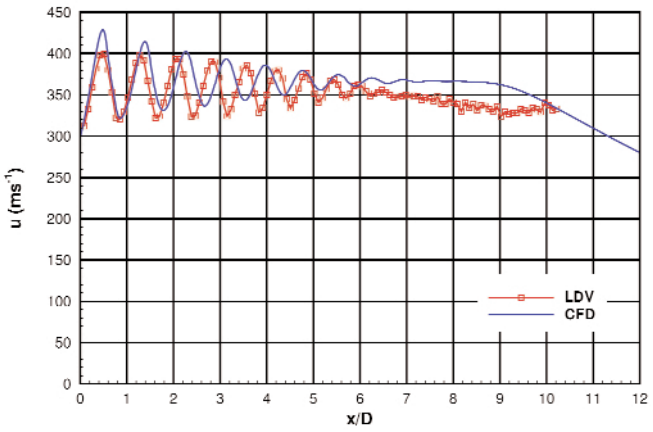

Figure11. Jet centreline axial velocity profiles, NPR = 2·5 – comparison of CFD and LDV.

3.0 RESULTS AND DISCUSSION

The results from the CFD model were compared with the LDV and pitot probe experimental measurements as discussed below.

3.1 Centreline axial velocity measurements

Figure 11 shows the variation in centreline axial velocity with *x/D* for the LDV and CFD data at a NPR of 2·5. The data agree reasonably well in terms of shock strength and location. A close examination of the LDV data indicated that ten shock cells had been captured. Shock cell length was defined as the distance between subsequent velocity peaks. The CFD model predicted the same ten shock cells that were captured by the LDV technique, however, it predicted slightly longer individual cells.

The shock core length, defined as the axial distance to the end of the last shock cell, could also be determined. At this pressure ratio, the shock core length is slightly over-predicted by the CFD, the end of the tenth cell occurring at *x/D* = 7·5 rather than *x/D* = 6·5, which

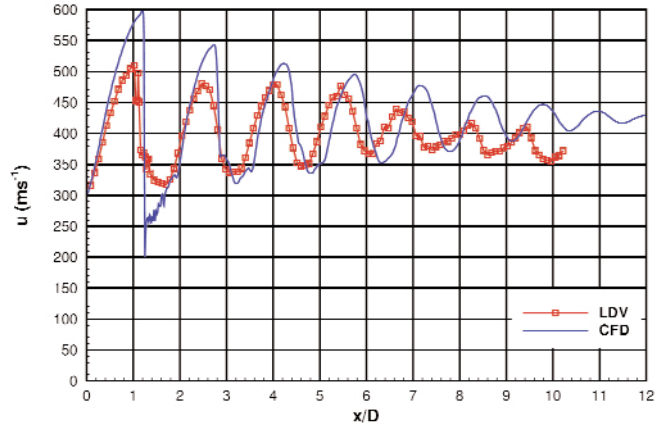

Figure 12. Jet of centreline axial velocity profiles, NPR = 4 – comparison of CFD and LDV.

Table 2
Comparison of shock cell lenghs for CFD, LDV and pitot probe techniques

	Shock cell length, *x/D*					
	NPR = 2·5			NPR = 4		
Cell	CFD (< ±0·005)	LDV (< ±0·042)	Pitot (< ±0·034)	CFD (< ±0·005)	LDV (< ±0·042)	Pitot (< ±0·034)
1	0·49	0·51	0·48	1·20	1·02	1·29
2	0·91	0·77	0·88	1·53	1·45	1·23
3	0·87	0·80	0·82	1·49	1·53	1·50
4	0·87	0·73	0·82	1·53	1·45	1·50
5	0·83	0·77	0·75	1·39	1·19	1·36
6	0·81	0·72	0·75	1·40	1·62	No data
7	0·76	0·59	0·61	1·23	1·19	No data
8	0·70	0·60	No data	1·18	No data	No data
9	0·68	0·51	No data	1·01	No data	No data
10	0·59	0·51	No data			

https://doi.org/10.1017/S0001924000151590 Published online by Cambridge University Press

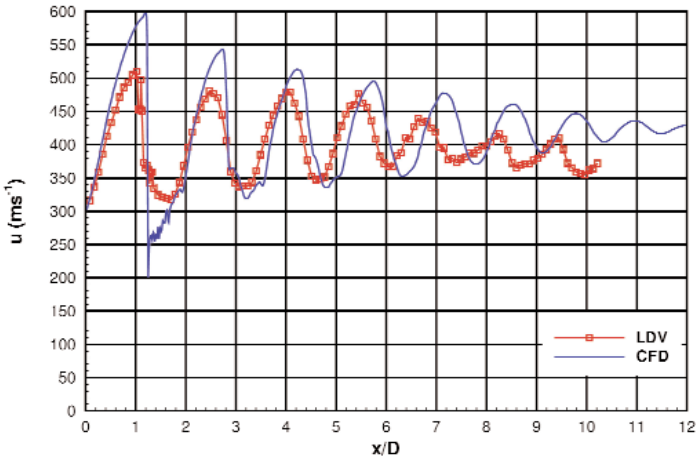

Figure 12. Jet centreline axial velocity profiles, NPR = 4 – comparison of CFD and LDV.

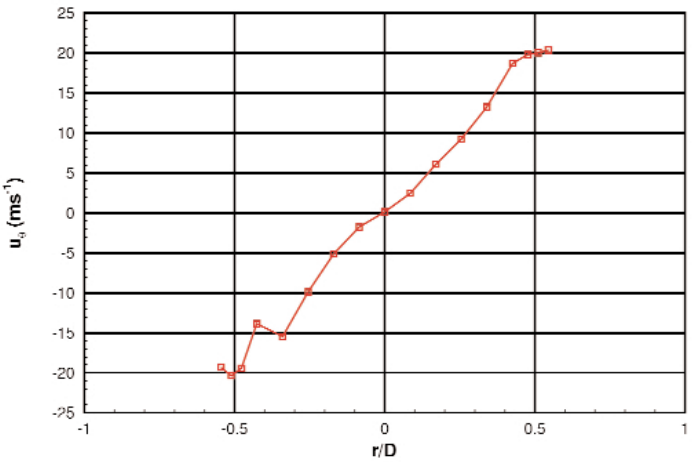

Figure 15. LDV-measured tangental velocity profile, NPR = 2·5, x/D = 0·085.

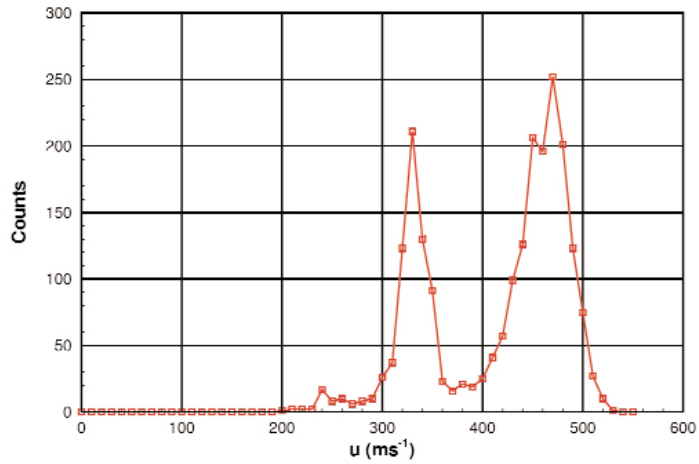

Figure 13. Distribution of sampled axial velocity, NPR = 4, x/D = 7 235.

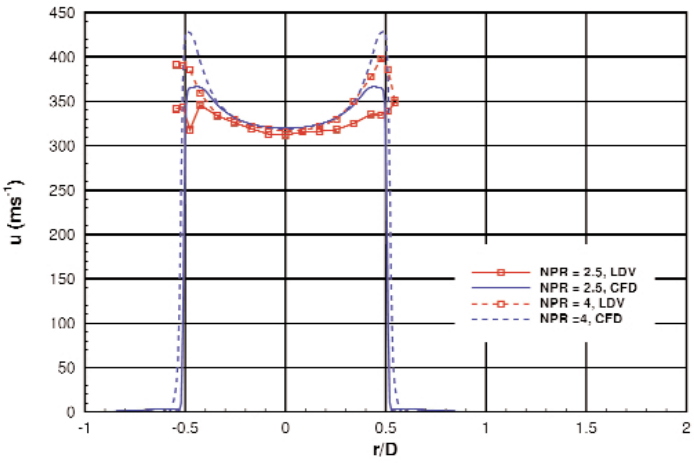

Figure 16. Jet radial velocity profiles, x/D = 0·085 – comparison of CFD and LDV.

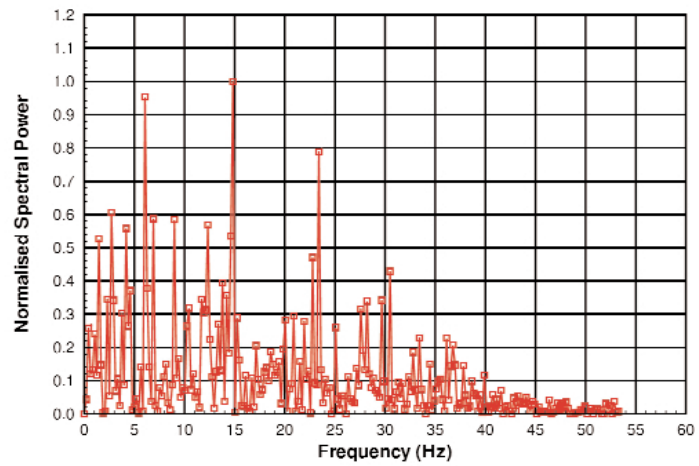

Figure 14. Frequency spectra for one LDV data point, NPR = 4, x/D = 7·235.

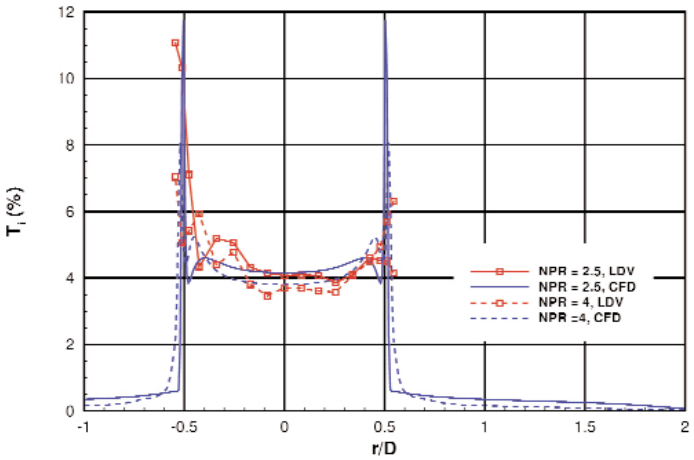

Figure 17. Jet radial turbulence intensity profiles, x/D = 0·085 – comparison of CFD and LDV.

https://doi.org/10.1017/S0001924000151590 Published online by Cambridge University Press

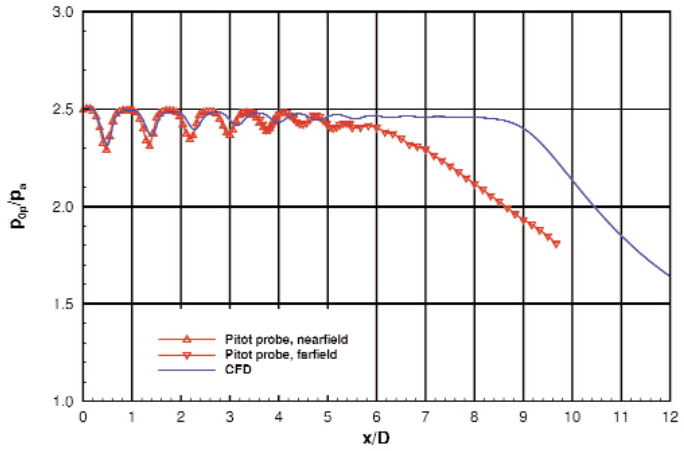

Figure 18. Jet centreline pressure profiles, NPR = 2·5 – comparison of CFD and pitot probe.

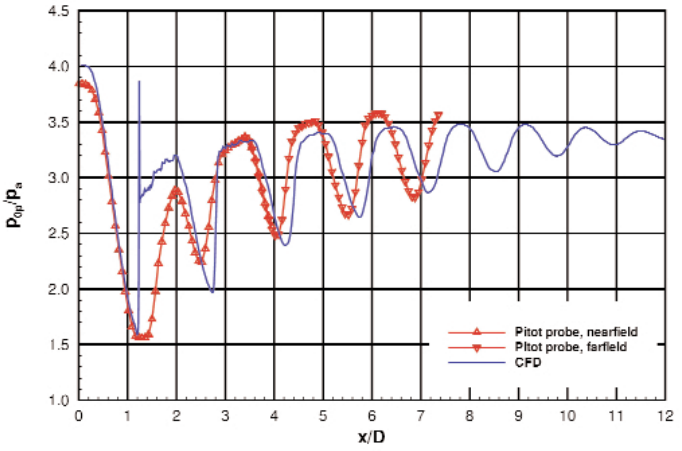

Figure 19. Jet centreline pressure profiles, NPR = 4, – comparison of CFD and pitot probe.

was measured by LDV. The supersonic core is predicted by the CFD to extend to x/D = 10·8 at which point the axial velocity is 316ms^{-1}. The end of the supersonic core is, however, not captured by the LDV traverse although there is some evidence of the onset of decay.

Increasing the NPR to 4 gives a substantial increase in the shock cell length (Fig. 12), as would be expected. Again the agreement between the CFD and LDV data is reasonable. Nine shock cells are captured by the CFD but the model is still over-predicting the cell length although not as much as in the NPR = 2·5 case. The LDV measurements appear to have peak velocities that are up to 15% less than the peak CFD velocities, particularly in the first few shock cells. The peak velocity in the CFD calculation is 599 ms^{-1} at x/D = 1·2. A correlation for the centreline Mach number in the core of underexpanded jets[14] predicts a velocity of 594ms^{-1}. The excellent agreement between these two predictions suggests, therefore, that the LDV measurements are in error.

The majority of the error can be accounted for by considering the seeding characteristics in response to an exponential acceleration [15]. With seeding diameters of between 0·5µm and 1·0µm, a particle density of 800kgm^{-3} and an exponential acceleration from 300 ms^{-1} to 600ms^{-1} in one nozzle diameter, the particle Stokes number will range from 0·01 to 0·05. This corresponds to a predicted particle lag error of between 5% and 15%.

A typical velocity distribution from the LDV data taken downstream in the jet, (Fig. 15) was characterised by a 'double peak', indicating that the jet was oscillating. This double distribution would result in an underestimation of the jet centreline velocity. How large an underestimation, however, is not known. The jet oscillation is thought to be due to impingement on the collector resulting in a low frequency oscillation[16] with a Strouhal number of the order of 0·01. A fast fourier transform of the data revealed the peak frequency of jet oscillation to be approximately 15Hz (Fig. 14). A similar effect could be created if the NPR were pulsing, causing the measurement point to be passing alternately through a peak and trough in the centreline velocity distribution. This is unlikely for a number of reasons. Firstly, the double peak in the LDV data was recorded at a number of streamwise positions. It would be highly coincidental if this corresponded to peaks and troughs in the velocity distribution. Secondly the NPR fluctuation would have to be large (of the order of ±15%), which was considered unlikely. Finally, the frequency of oscillation is an order of magnitude lower than the characteristic frequency of the compressor machinery, which is a continuous displacement machine rotating at 6,000rpm.

A radial traverse close to the nozzle exit plane (x/D = 0·085) also established the existence of a 20ms^{-1} peak swirl velocity (Figure 15). Swirl has been shown to shorten the shock cell length in supersonic jets[17]. The extent to which swirl might affect the results presented here is not known, however the swirl angle of approximately 3·2°. at the jet periphery was thought to be sufficiently large to affect the jet decay. The combination of swirl and jet oscillation (described above) might be responsible for the apparently reduced shock cell length in the experiment as compared with the CFD model. Even after taking these effects into consideration, however, the CFD model shows better agreement with the experimental data than has been previously reported[18].

A summary of the shock cell lengths for the CFD, LDV and pitot probe measurements (discussed below) is given in Table 2. Tolerances are quoted at the top of each column which indicate the resolution of the experimental measurements and CFD mesh.

3.2 Radial velocity measurements

Radial velocity measurements were also made using the LDV technique. Measurements made close to the nozzle exit plane (x/D = 0·085) show good agreement between the LDV-measured and CFD-predicted velocity profiles (Fig. 16). Both the LDV and CFD data show the characteristic velocity deficit at the centre of the jet, which is due to a 'bowing' of the sonic line at the nozzle exit.

Radial profiles of turbulence intensity (Fig. 17) also show good agreement. The centreline data agree well as would be expected, since the CFD was set up to match the experimental value here. The plots also show good agreement between CFD and experiment in the higher turbulence intensity regions found in the jet shear layer.

3.3 Centreline pitot probe measurements

The pitot probe data, p_{0p} were non-dimensionalised with ambient static pressure, p_a and plotted against non-dimensional axial distance, x/D along the nozzle centreline. Corresponding centreline static pressure measurements were not made, however, which meant that the usual Rayleigh correction for a stand-off normal shock in front of the probe could not be applied. In order to compare the pitot probe data with the CFD model, the CFD-predicted static pressure and Mach number were used in the normal shock equation (Equation 1).

$$\frac{p_{02}}{p_1} = \left[\frac{(\gamma+1)M_1^2}{2}\right]^{\frac{\gamma}{\gamma-1}} \left[\frac{\gamma+1}{2\gamma M_1^2-(\gamma-1)}\right]^{\frac{1}{\gamma-1}} \quad \ldots(1)$$

where the subscripts '1' and '2' indicate conditions upstream and downstream of a normal shock respectively.This effectively gives the total pressure that a pitot probe would see if placed in the CFD-predicted flow field (assuming a stand-off normal shock). Figures 18

https://doi.org/10.1017/S0001924000151590 Published online by Cambridge University Press

and 19 present pitot probe traverse data and CFD data for NPRs of 2·5 and 4 respectively. Each set of pitot probe data is in two parts, labelled 'nearfield' and 'farfield', resulting from the enforced relocation of the traverse carriage. The overlap between the nearfield and farfield results is an indication of the repeatability of the pitot probe data.

A comparison of the data for a NPR of 2·5 (Fig. 18) shows very good agreement in the initial shock cells. The nozzle exit pressure ratio of 2·5 is captured by both methods and the variation in pressure ratio through the shock system is in good agreement. The pitot probe data capture only seven shock cells compared to the ten predicted by the CFD. The pitot probe measurements indicate that the shock cells are shorter than the CFD prediction, which is in agreement with the LDV measurements.

The main difference between the two sets of data is in the supersonic core length, which appears somewhat shorter in the pitot probe data. This was originally thought to be most likely due to differences in the jet conditions between the experimental set-up and the CFD model, however, the possibility of probe interference must also be considered as a contributory factor. The LDV data indicates that the jet becomes subsonic at $x/D \approx 10$, characteristic of previous experiments[5], and slightly earlier than the CFD prediction of 10·8D. The pitot probe data indicates a subsonic jet exists at $x/D \approx 9{\cdot}3$, a more rapid decay. The two sets of experimental data were taken under nominally the same conditions, the only difference being the intrusive nature of the pitot probe. Stickland[5] also considered the possibility of probe interference in their data after analysis of schlieren images indicated that the probe caused substantial distortion of the shock cell structure. It is felt that some probe interference in Wong's data[9-10] in combination with jet oscillation and exit swirl has caused earlier than anticipated decay of the jet.

At the higher NPR (Fig. 19) agreement between the pitot probe measurements and the CFD model are again good. The CFD data indicates the formation of a small Mach disc which is characterised by the region of subsonic flow on the centreline after the first shock cell. The pitot probe measurements do not show the small Mach disc, which is predicted by the CFD model, however the shock strengths downstream of the first cell agree very well. The exit pressure ratio on the experimental data is slightly below the set value, however, it is not known whether this is a real effect or a probe interference problem. Unfortunately, the experimental measurements were not able to capture the whole of the shock core but the indications are that the CFD model is over-predicting the shock cell lengths, as concluded from the LDV discussions (see Table 2).

CONCLUSIONS

A study has been presented of under-expanded axisymmetric turbulent jets. A CFD calculation using the RNG κ–ε turbulence model and solution-based mesh adaption has been shown to capture all the main features of the nearfield flow up to 10 nozzle diameters downstream of the exit plane. Comparison with experimental LDV and pitot probe measurements indicates that the CFD model is predicting shock cells that are too long. There is evidence, however, that the experiments are suffering from premature jet decay caused by a combination of swirl in the jet flow, jet unsteadiness and, in the case of the pitot measurements, some probe interference.

REFERENCES

1. PINKER, R.A. and STRANGE, P.J.R. The noise benefits of forced mixing, proceedings of the 4th AIAA/CEAS Aeroacoustics Conference, Toulouse, France, 2-4 June 1998, Paper No. AIAA-98-2256.
2. BEVILAQUA, P.M. Advances in ejector thrust augmentation, Proceedings of the International Powered Lift Conference, Santa Clara, California, USA, 7-10 December 1987, pp 201–215.
3. RAO, G.A. and MAHULIKAR, S.P. Integrated review of stealth technology and its role in airpower, *Aeronaut J*, December 2002, **106**, (1066), pp. 629–641.
4. DONALDSON, C.D. and SNEDEKER, R.S. A study of free jet impingement. Part 1. mean properties of free and impinging jets, *J Fluid Mechanics*, 1971, **45**, (2), pp 281–319.
5. STICKLAND, M.T. RA98 (CHAM Nozzle) Flow survey of under-expanded supersonic jets in the 5·5m low speed wind tunnel static test facility – Volume 2, Technical Report BAe-WWT-RPRES-AXR-139, BAe plc., April 1988.
6. KALGHATGI, G.T., COUSINS, J.M., and BRAY, K.N.C. Crossed beam measurements and model predictions in a rocket exhaust plume, combustion and flame, 1981, **43**, pp 51–67.
7. CHUECH, S.G., LAI, M.C., and FAETH, G. M. Structure of turbulent sonic underexpanded free jets, *AIAA J*, May 1989, **27**, (5), pp 549–559.
8. LOVE, E.S., GRIGSBY, C.E., LEE, L.P. and WOODLING, M.J. Experimental and theoretical studies of axisymmetric free jets, Technical Report R-6, NASA, 1958.
9. KNOWLES, K. and WONG, R.Y.T. Passive control of entrainment in supersonic jets, RAeS Aerodynamics Research Conference, London, 17-18 April 2000, pp 9.1–9.14.
10. WONG, R.Y.T. Enhancement of supersonic jet mixing, PhD thesis, Department of Aerospace, Power and Sensors, Cranfield University, July 2000.
11. RODI, W. Turbulence models and their application in hydraulics – A state of the art review, International Association for Hydraulic Research, Rotterdamseweg 185 – PO Box 177, 2600 MH Delft, The Netherlands, 2nd ed., 1984.
12. YAKHOT, A. and ORSZAG, S.A. Renormalisation group analysis of turbulence: I. Basic theory, *J of Scientific Computing*, 1986, **1**, (1), pp 1–51.
13. KNOWLES, K. and SADDINGTON, A.J. Modelling and experiments on underexpanded turbulent jet mixing, 5th International Symposium on Engineering Turbulence Modelling and Measurement, Mallorca, Spain, 16-18 September 2002.
14. ASHKENAS, H. and SHERMAN, F.S. Structure and utilization of supersonic free jets in low density wind tunnels, Contractor Report CR-60423, NASA, 1964.
15. DRING, R. P. Sizing criteria for laser anemometry particles, *J Fluids Engineering*, 1982, **104**, pp.15–17.
16. ROCKWELL, D. Oscillations of impinging Shear Layers, *AIAA J*, 1983, **21**, (5), pp. 645–664.
17. SMITH, R. An Investigation of supersonic swirling jets, *Aeronaut Q*, August 1973, **24**, pp 167–178.
18. BIRKBY, P. and PAGE, G.J. Numerical predictions of turbulent underexpanded sonic jets using a pressure-based methodology, Proceedings of the Institution of Mechanical Engineers, 2001, **215**, (G), pp 165–173.

https://doi.org/10.1017/S0001924000151590 Published online by Cambridge University Press